AGU PUBLICATIONS

Water Resources Research

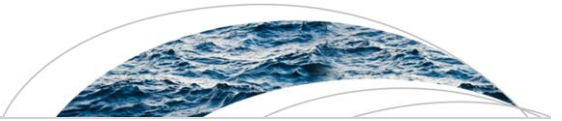

RESEARCH ARTICLE

10.1002/2014WR015858

Key Points:
- Subsecond displacement is studied with fast X-ray microcomputed tomography
- Fluid front propagates as cascade-like events that are tracked in time and space
- Image quality of reconstructed data is improved with presented approach

Supporting Information:
- Readme
- Figure S01

Correspondence to:
R. T. Armstrong,
ryan.armstrong@unsw.edu.au

Citation:
Armstrong, R. T., H. Ott, A. Georgiadis, M. Rücker, A. Schwing, and S. Berg (2014), Subsecond pore-scale displacement processes and relaxation dynamics in multiphase flow, *Water Resour. Res.*, *50*, 9162–9176, doi:10.1002/2014WR015858.

Received 18 MAY 2014
Accepted 7 NOV 2014
Accepted article online 13 NOV 2014
Published online 1 DEC 2014

Subsecond pore-scale displacement processes and relaxation dynamics in multiphase flow

Ryan T. Armstrong[1], Holger Ott[2], Apostolos Georgiadis[2], Maja Rücker[3], Alex Schwing[2], and Steffen Berg[2]

[1]School of Petroleum Engineering, University of New South Wales, New South Wales, Sydney, Australia, [2]Shell Global Solutions International B.V., Rijswijk, Netherlands, [3]Geosciences Institute, Johannes Gutenberg University, Mainz, Germany

Abstract With recent advances at X-ray microcomputed tomography (μCT) synchrotron beam lines, it is now possible to study pore-scale flow in porous rock under dynamic flow conditions. The collection of four-dimensional data allows for the direct 3-D visualization of fluid-fluid displacement in porous rock as a function of time. However, even state-of-the-art fast-μCT scans require between one and a few seconds to complete and the much faster fluid movement occurring during that time interval is manifested as imaging artifacts in the reconstructed 3-D volume. We present an approach to analyze the 2-D radiograph data collected during fast-μCT to study the pore-scale displacement dynamics on the time scale of 40 ms which is near the intrinsic time scale of individual Haines jumps. We present a methodology to identify the time intervals at which pore-scale displacement events in the observed field of view occur and hence, how reconstruction intervals can be chosen to avoid fluid-movement-induced reconstruction artifacts. We further quantify the size, order, frequency, and location of fluid-fluid displacement at the millisecond time scale. We observe that after a displacement event, the pore-scale fluid distribution relaxes to (quasi-) equilibrium in cascades of pore-scale fluid rearrangements with an average relaxation time for the whole cascade between 0.5 and 2.0 s. These findings help to identify the flow regimes and intrinsic time and length scales relevant to fractional flow. While the focus of the work is in the context of multiphase flow, the approach could be applied to many different μCT applications where morphological changes occur at a time scale less than that required for collecting a μCT scan.

1. Introduction

X-ray microcomputed tomography (μCT) is ideal for imaging the spatial arrangement of static immiscible fluids in porous rock at micrometer resolution [e.g., *Al-Raoush*, 2009; *Wildenschild et al*., 2002, 2005; *Pentland et al*., 2010; *Iglauer et al*., 2011]. However, it is critical that the scanned object does not change substantially during the scan period and therefore most experiments are imaged at equilibrium or quasi equilibrium. Not until recently have scan times become rapid enough to image the movement of immiscible phases under dynamic flow conditions, e.g., as demonstrated by *Berg et al*. [2013a]. To understand why this works and what the possibilities are for imaging the movement of immiscible phases in porous rock, we first give a brief technical introduction on μCT followed by a comparison between the time scales relevant to μCT and those relevant to pore-scale multiphase flow and then we propose an approach to study subsecond flow processes with μCT.

For μCT, a sample is placed on a rotational stage and exposed to an X-ray beam, radiation passes through the sample and is then converted into visible light via a scintillator. The visible light is magnified by optical lenses and projected onto a charge-coupled device (CCD) image sensor. The resulting 2-D image, referred to as a radiograph, is a linear attenuation map of the sample at a given rotational angle. With a collection of radiographs over a sample rotation of either 180° or 360° degrees, depending on X-ray beam geometry, a reconstruction algorithm can be used to produce a 3-D map of attenuation coefficients that represent the physical structure of the imaged sample. This technique requires that the sample remains static during the scan time otherwise imaging artifacts could occur. Depending on X-ray flux and other system capabilities, the entire scan time (time required to collect a 3-D image) could range from hours to seconds since many radiographs at different rotational angles are required for image reconstruction and each radiograph requires an exposure time of milliseconds to seconds. For synchrotron-based μCT, high X-ray flux is supplied

by the synchrotron and thus, the entire scan time can take only a few seconds since the exposure time of a single radiograph is milliseconds. The only major limitation with this approach is the data read-out time from the CCD. In comparison, a major limitation with bench top μCT systems is that scan times are usually on the order of hours since the radiograph exposure time is often many seconds because of low X-ray flux. However, *Myers et al*. [2011] were able to reduce the scan time of a bench top μCT system to minutes by using a discrete tomography approach that allowed for a significant reduction in the number of required radiographs. Overall, for bench top or synchrotron-based μCT systems, the time required to collect a single radiograph (radiograph exposure time) multiplied by the number of radiographs required to reconstruct a 3-D image will set the lower temporal limit for the type of processes that can be imaged in 3-D.

Recent advances at μCT synchrotron beam lines, such as the TOMCAT beam line at the Swiss Light Source, have decreased scan time (time required to collect a 3-D image) to seconds. These advances provide an excellent opportunity to study dynamic processes, such as multiphase flow through porous media. The most recent publications using fast-μCT data to study porous media flows are *Berg et al*. [2013a, 2013b], *Armstrong et al*. [2014], *Youssef et al*. [2013], and *Koroteev et al*. [2013]. However, it is unclear how pore-scale multiphase flow processes can be imaged with fast-μCT since some pore-scale flow processes occur at the millisecond time scale, which is equivalent to the time required to collect a single radiograph (exposure time). For example, local fluid velocities orders of magnitude greater than the expected Darcy velocity can occur during drainage when interfaces pass through pore bodies (R. T. Armstrong, et al., Velocity field during Haines jumps in porous media, submitted to *Advanced Water Resources*, 2014b). Because of these interfacial jumps, commonly referred to as Haines jump [*Haines* 1930], the interfacial dynamics during drainage will not be resolved with fast-μCT. As described in *Morrow* [1970], these interfacial jumps are observed in pressure transducer readings as a rapid decrease in pressure followed by a gradual pressure rebound over a matter of seconds. This pressure drop is indicative of changes in the spatial arrangement of fluids in the pore space, which during a μCT scan can results in imaging artifacts in the reconstructed image (as will be demonstrated). One approach to reduce these artifacts is to lower the nonwetting phase injection rate. In micromodel experiments, we find that the rate of a Haines jump is unaffected by the fluid injection rate. Rather the injection rate only controls the jump frequency and therefore, we can reduce the number of jumps that occur during a fast-μCT scan by reducing the injection rate [*Armstrong and Berg*, 2013], which was the approach taken in our previous work.

Multiphase flow on the pore scale can be decomposed into a quasi-equilibrium step where the volume of nonwetting phase in liquid-liquid menisci is increased followed by a disequilibrium step where rapid fluid reconfiguration occur (Haines jump) and lastly sequential interfacial relaxation to a new quasi-equilibrium state [*Morrow*, 1970]. At field-relevant flow regimes where the fluid front advances by approximately 3.5×10^{-6} m/s (1 foot/day in typical oilfield units), there is a clear separation of time scales between the Haines jumps, interfacial relaxation, and the associated flow boundary condition, e.g., the "volumetric front" during constant rate injection. In a typical μCT flow experiment, conducted at a flow rate of 3.5×10^{-6} m/s via a constant rate injection pump, the volumetric fluid front advancement over the field of view of approximately 4 mm requires more than 1000 s. As will be shown in this paper, the time scale associated with the reconfiguration/relaxation is 0.5–2.0 s. That means that there is a clear separation of time scales between pore-scale displacement events and the flow boundary condition. However, at a scanning interval of 1–60 s, there is no clear separation of time scales between pore-scale displacement events and intervals during which radiographs are recorded for the tomographic reconstruction. Hence, the approach of considering only full reconstructed μCT data at a time resolution of 1–60 s is not robust enough to study more complex multiphase flow regimes where the number of Haines jumps during a full scan is likely large, e.g., fractional flow with ganglion dynamics [*Avraam and Payatakes*, 1995].

In this publication, we present a method to collect artifact free images during multiphase flow experiments followed by a method to extract a wealth of information from μCT data where no artifact-free data could be reconstructed because of frequent morphological changes during data collection (see supporting information for a diagram of the general concept). We first analyze the 2-D radiograph data collected during a fast-μCT scan to study fluid movement at the millisecond time scale and to identify "locations" in the radiograph data where the highest quality 3-D image can be reconstructed. The traditional approach with μCT is to collect radiographs over a sample rotation of 180° (for a parallel X-ray beam geometry), reconstruct the data, and then repeat. This allows for the collection of reconstructed 3-D images at a regular time interval,

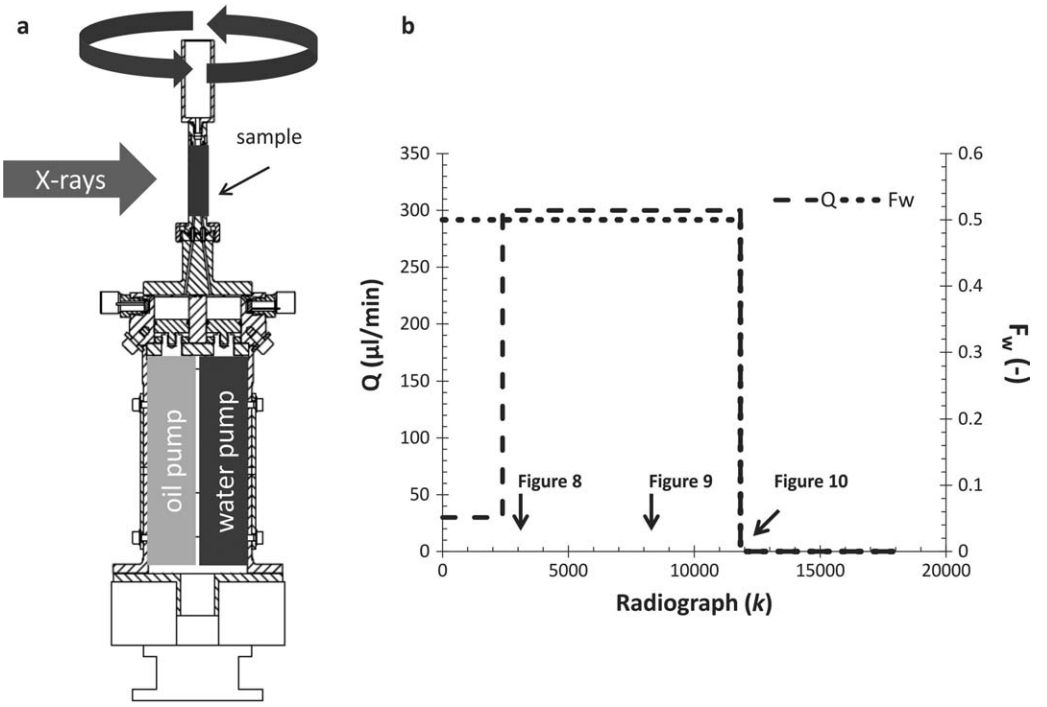

Figure 1. Dual pumps are located in the base of the μCT flow cell, which allows for the coinjection of fluids and continuous sample rotation (a). Radiographs (40 ms exposure) were continuously collected while the sample rotated at 0.25°/s. The rate of fluid injection was increased by an order of magnitude; while fractional flow remained constant at $F_w = 0.5$ (b). At two thirds of the total scan time, fluid injection was stopped.

corresponding to sample rotation of 180°. Conversely, reconstructed 3-D images could be collected at any given time interval, down to a minimum time interval equivalent to the exposure time of a single radiograph. This is accomplished by continuously collecting radiographs for the duration of an experiment, while the experimental setup continuously rotates. The output is a continuous array of radiographs, where each radiograph represents a moment in time. Then a "reading frame" that represents 180° degrees of sample rotation (a region of data that can be reconstructed, an explicit definition is provided in subsection 3.1) can be shifted to any given location in the radiograph array to read and sequentially reconstruct a 3-D image. We refer to shifting of the reading frame as a frame shift (see subsection 3.1) and the minimal shift possible is a single radiograph. However, not every possible frame shift for the collected data is ideal for the collection of artifact-free data. We propose the concept of a qualifier function that identifies the frame shift locations where the highest quality reconstruction exists. Moreover, the radiograph data between any two given frame shift locations can be analyzed to study fluid movement at a time scale equivalent to that required for collecting a single radiograph. With this approach, the 3-D data are supplemented with 2-D data that provides information on event size, order of events, event frequency, and event location. Overall, many different μCT-imaging applications where rapid morphological changes are expected could benefit from the presented method.

2. Materials and Methods

The μCT experiments were performed at the TOMCAT beam line at the Swiss Light Source, Paul Scherrer Institute, Villigen, Switzerland. We designed a flow cell with dual micropiston pumps integrated into the base of the sample holder (see Figure 1). The design allows for the coinjection of two fluid phases (e.g., oil and water) at different rates without any external flow lines. The pump operates similar to a syringe pump and is driven by a stepper motor. Each pump cylinder has an inner surface area of 201.1 mm^2 and length of 10 mm. The stepper motor operates at 384 μsteps/revolution with a pitch of 0.5 mm/revolution (maximum torque = 0.15 mNm), which results in a minimum flow rate of 0.043 μL/min. At the outlet of the pumps, Keller 2 Mi piezoresistive miniature sensors were mounted for monitoring pressure at a sampling rate of 10 Hz.

Table 1. Settings Used at the TOMCAT Beam Line

Option	Setting	Option	Setting	Option	Setting
Energy	36 keV	OP-filter 2	40 μm Cu	Angular step	0.12
FE-filter	50%	OP-filter 3	10 μm Fe	Radiographs	1500
OP-filter 1	100 μm Al	Exposure time	40 ms	Lens magnification	3.08x
Camera	PCO.EDGE	Pixel size	2.11 μm	Scintillator	100 μm thick cerium-doped lutetium aluminum garnet

The transducers have a pressure range of 0–5 bar (gauge pressure). Data acquisition was accomplished using a radio frequency transmitter mounted on the base of the flow cell. All of the electronics mounted to the flow cell were powered through a slip-ring connection that is available on the sample stage at the TOMCAT beam line. With this design, a constant output of radiographs can be collected during a multiphase flow experiment since the sample can continuously rotate.

The presented μCT data are from a fractional flow experiment conducted using a model porous media system. The porous sample was Robuglas® ($\phi = 31.8\%$, $k = 8.9 \times 10^{-12}$ m^2, $diameter = 4$ mm, $length = 10$ mm) and the immiscible fluids were water (14.3% by weight CsCl) and n-decane. The experiment was initiated by the coinjection of fluids at a ratio of 1:1 ($F_w = 0.5$, see Figure 1) with a total injection rate of 30 μL/min. Once the pressure reading stabilized the continuous collection of radiographs was initiated. The radiographs represent a small field of view (5.4 × 4.6 mm) along the vertical center of the sample. Therefore, 2.7 mm of the inlet and outlet regions of the sample were not imaged and hence the exact flow boundary conditions for the field of view are unknown (they are neither constant flow nor constant pressure, see *Morrow*, [1970]; *Berg et al*. [2013]). Total injection rate was increased to 300 μL/min near radiograph 2500 and then the system was allowed to equilibrate, followed by stopping of the pumps near radiograph 12,000 (Figure 1b). The settings used at the TOMCAT beam line are presented in Table 1. With these settings, a reading frame of data that can be reconstructed consists of 1500 projections and the minimum frame shift is equivalent to 40 ms (or 1 radiograph). A total of 18,012 radiographs were collected for a total data collection time of approximately 12 min. The radiographs were normalized with Octopus image reconstruction software (Inside Matters, Aalst, Belgium) to adjust for slight fluctuations in X-ray beam intensities during the scan period. Python(*x, y*) 2.7.6.0 (python.org) with Matplotlib and NumPy libraries were used to analyze the radiographs, test the proposed qualifier function, and measure the spatial frequencies (power spectrum) of the collected radiographs. Last, a FFT band-pass filter provided in ImageJ (National Institute of Health, Maryland, USA) was used for filtering the radiograph data and Avizo Fire 8.0 (Visualization Sciences Group, FEI Instruments) was used for segmentation of the filtered data.

3. Results and Discussion

The Results and Discussion are divided into three subsections: 3.1 Qualifier Function, 3.2 Time Scales (*k*), and 3.3 Fluid Flow. In subsection 3.1, a qualifier function is introduced that measures the difference in sequential radiographs and thus, indicates intervals in time when large morphological changes occur. In subsection 3.2, we analyze over what time scale should differences in sequential radiographs be measured and demonstrate approaches/settings for the qualifier function that do and do not work for identifying regions in the radiograph data where high-quality 3-D images can be reconstructed. In subsection 3.3, we explore regions in the radiograph data where no high-quality data could be reconstructed because of frequent morphological changes of fluid-fluid interfaces by pore-scale displacement events. By analyzing sequential radiographs, we are able to study fluid flow processes at the millisecond time scale and extract information not obtainable from the 3-D reconstructed data that is available only at time scales of 1 s and longer. In general, with μCT experiments the radiograph data are not often used to study the flow physics. However, as demonstrated herein, the radiograph data can provide many valuable insights into the flow physics and should not be overlooked and could be used to supplement the 3-D reconstructed data.

3.1. Qualifier Function

During the experiment, we collect a continuous array of radiographs (I_k) where the subscript (*k*) denotes the radiograph number. For a constant data collection time per radiograph (*E*, exposure time), the total elapsed

time of the experiment is $k \times E$ and the time elapsed between any two radiographs I_{k1} and I_{k2} is $(k2 - k1) \times E$. A reading frame can be defined as a collection of sequential radiographs that constitutes 180° of sample rotation (1500 radiographs for the presented data). This reading frame can be shifted to any given location k within I_k to reconstruct a 3-D image and we refer to this movement as a frame shift. The location of the frame shift is defined by the location k of the first radiograph used for the image reconstruction. With this approach, where the maximum number of collected radiographs is defined by $k_{max,}$ a total of $k_{max} - 1499$ image reconstructions are possible since the reading frame can be shifted by as little as one radiograph once enough radiographs to constitute a reading frame are collected. However, the reconstruction of all possible frame shift locations is neither reasonable nor required. Rather, we propose the concept of a qualifier function that would quantify the amount of fluid movement that occurs within a reading frame at any given frame shift prior to image reconstruction. The qualifier function versus frame shift dimension could then be searched for locations with an absence of fluid moment in the reading frame, i.e., where the highest quality 3-D images could be reconstructed. The basis for such a qualifier function is to compute differences between radiographs taken at different times to locate regions where the least amount of change occurs.

For the qualifier function we propose an equation with the following functional form

$$\bar{Q}_k(k,z) = \frac{\sum_i \sum_j |I[i,j]_k - I[i,j]_{k+z}|}{n} \tag{1}$$

where I is a 8-bit gray-scale radiograph image (2-D matrix of measured X-ray intensity values) with dimensions $[i, j]$ and n is the total number of pixel elements ($i \times j$). Therefore, $\bar{Q}_k$ is the forward piecewise average absolute difference of pixel intensity values between radiograph k and $k + z$ and by adjusting z we can control the time scale over which differences are considered (e.g., with $z = 2$ then equation (1) would measure changes over a $2 \times E$ time scale or 80 ms for the presented data). As z is increased, the differenced images $(|I_k - I_{k+z}|)$ are not necessary sensitive to only fluid movement since the projected pore space also changes. However, we explore only special cases where z is either small or I_{k+z} represents a mirror image of I_k. In the following section, we discuss the z values that lead to a more successful indication of displacement events and which did not. The results of which also gives insight into the time scales relevant to pore-scale flow since z sets the time scale over which changes are considered. With equation (1), the absolute difference was computed and we therefore do not distinguish between water displacing oil or conversely oil displacing water.

Once $\bar{Q}_k$ is calculated for a set of radiographs then a running average can be calculated to locate regions within the data that result in a minimum value. The idea is to calculate the running average over a region of $\bar{Q}_k$ values that represent a region of data that can be reconstructed (reading frame) and therefore, minimum values should correspond to frame shift locations where the amount of fluid movement during a scan was minimal. The running average is defined such that it represents an average $\bar{Q}_k$ for any given frame shift (k) within the radiograph data

$$\langle \bar{Q} \rangle_k = \sum_{k-s/2}^{k+s/2} \frac{\bar{Q}_k}{s} \tag{2}$$

where s is the total number of radiographs required to reconstruct a 3-D image ($s = 1500$ for the presented data). Therefore, minimum values of $\langle \bar{Q} \rangle_k$ would correspond to regions in the radiograph array (I_k) at location k where a reading frame should be shifted to for image reconstruction. In other words, $\langle \bar{Q} \rangle_k$ is the convolution of $\bar{Q}_k$ over a region of reconstructible data. Relatively large $\langle \bar{Q} \rangle_k$ values should correspond to periods in time with relatively large morphological changes (fluid flow), whereas relatively small $\langle \bar{Q} \rangle_k$ values correspond to periods in time with relatively small morphological changes (no fluid flow).

3.2. Time Scales (z)

Initially, we considered the case of $z = 1500$, which corresponds to a total sample rotation of 180° and a time scale of 60 s. For this case, images I_k and I_{k+z} are mirror projections and this was accounted for by reflecting I_{k+z} over its central y axis prior to applying equation (1). When no morphological changes occur, it is expected that the resulting average difference in radiographs would be small and be of the order of the noise level in the data. However, even when morphological changes occur $\bar{Q}_k$ is also relativity small since it is an average value and the regions in the radiograph data where change occurs are relatively small in comparison to regions where no change occurs. The proposed qualifier function, pressure data collected during

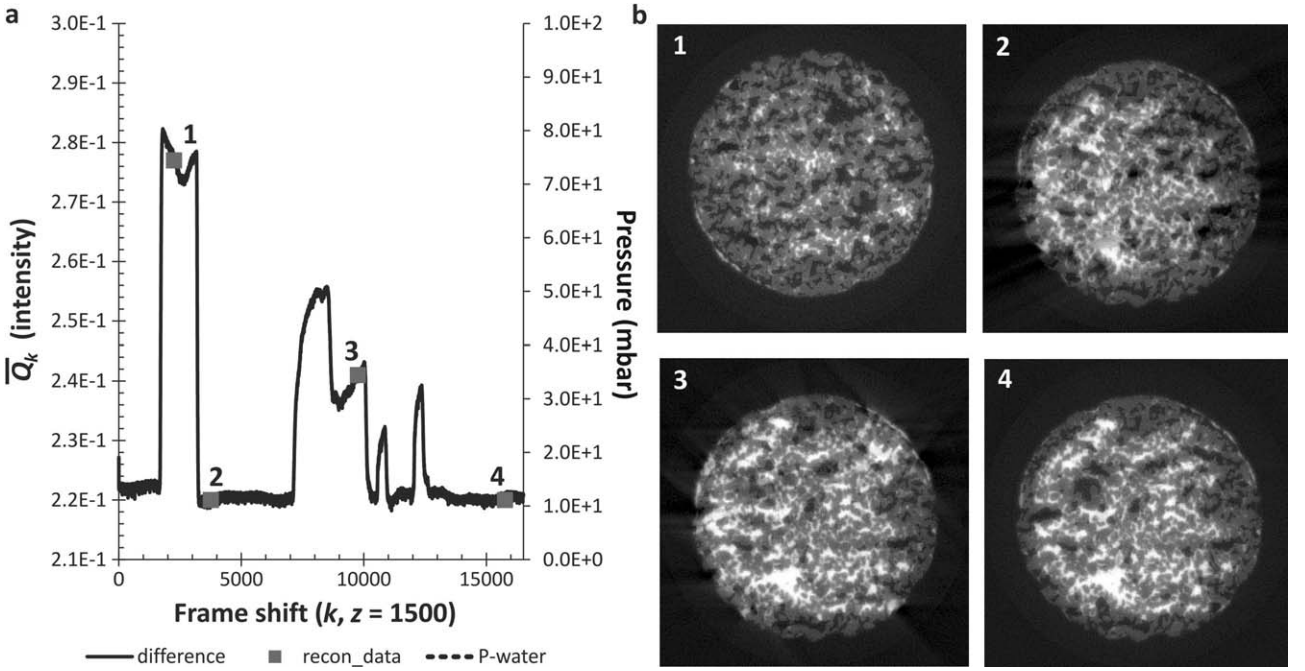

Figure 2. $\bar{Q}_k$ (with $z = 1500$) correlates well with the oil and water pressure transducer data. However, for a given reconstruction volume, there is no correlation between the quality of the reconstructed data and $\bar{Q}_k$. Presumably, difference in data over the second time scale (with $z = 1500$) is too large of a time period since pore-scale displacement is known to occur at the millisecond time scale.

the experiment, and examples of reconstructed data are presented in Figure 2. For this case, $\langle \bar{Q} \rangle_k$ was not calculated since $\bar{Q}_k$ with $z = 1500$ is equivalent to a region of data that can be reconstructed. Streaking artifacts caused by fluid movement during a scan are apparent in Figure 2b in reconstructed volumes 2 and 3, whereas reconstruction volumes 1 and 4 resulted in streak-free data. The streaking artifact is presented in more detail in Figure 3 where regions of interest from volumes 1 and 2 from Figure 2 are presented. This streaking artifact is difficult to remove in post processing and consequently leads to artifacts when segmenting the image into the different phases (oil, water, and rock). Please note that in the images in Figures 2 and 3 an additional blurring artifact is visible which is not related to fluid motion during scanning intervals. The blurring artifact occurs over the interface between the high attenuating fluid (water) and the porous structure (glass). However, this is likely caused by phase contrast issues (not the result of fluid movement) and can be accounted for by collecting an initial dry image of the porous material whereas the streaking artifact is not as easily circumvented.

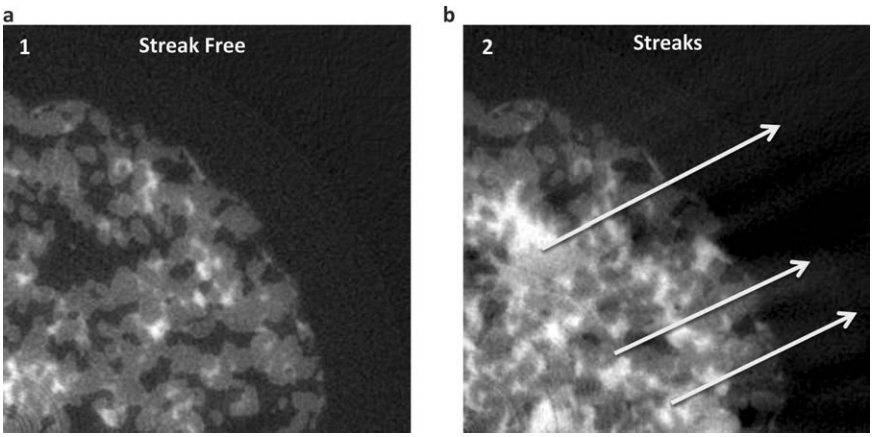

Figure 3. More detailed view of reconstruction volumes 1 and 2 presented in Figure 2b. Volume 1 has no streaking artifacts (a) whereas volume 2 (b) has high intensity streaks across the image (as labeled by the white arrows).

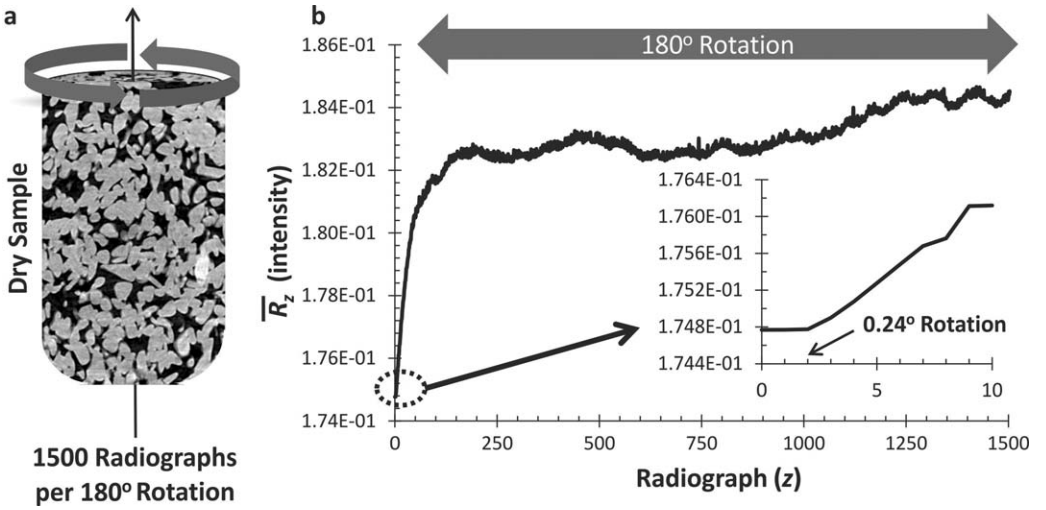

Figure 4. For data collected on a dry sample, $\bar{R}_z$ is relatively small for a time span of ~200 ms ($z = 5$). Therefore, the radiograph data can be sampled using equation (1) with $z < 5$ (differenced at a much higher rate similar to the rate of individual fluid-fluid displacement events).

No correlations between the pressure transducer and/or the qualifier function data and the reconstructed data quality are noticeable. For example, reconstruction volume 1 corresponds to a frame shift location with a relatively large $\bar{Q}_k$ value even though the resulting data has no streaking artifacts. Conversely, reconstruction volume 4 corresponds to a frame shift location with a relatively small $\bar{Q}_k$ value and the resulting data also has no blurring artifacts. It is clear that equation (1) with $z = 1500$, is not sensitive enough to identify the morphological changes that result in the observed image blurring artifacts. One possible explanation is that even if bulk morphology does not change over the duration of a scan, small local morphological changes or fluctuations during the scan could cause the streaking artifact. This would of course depend significantly on the fractional flow conditions, e.g., connected phase flow versus ganglion dynamics or front propagation, as discussed later.

To evaluate the possibility that the blurring artifacts are caused by morphological changes over a time scale less than a single scan, we decided to evaluate the average difference between radiographs over a much shorter time scale, i.e., $z < 1500$. In the previous example, we were able to measure differences over the time required to rotate the sample 180° since radiographs at 0° and 180° are mirror images and therefore, any measured difference would be the result of fluid movement. However, now that average differences are to be measured for $z < 1500$, differences in the projected pore structure will also be measured. However, we expect this difference to be minimal for small z since this corresponds to a small degree of sample rotation and there should be some level of similarity in the collected radiographs. To quantify this, we imaged the dry Robuglas® sample (where no changes in the sample itself can occur, i.e., there are no fluids and hence there can be no change due to fluid displacement) and measured ($\bar{R}_z$) the difference between the 1st and zth radiographs in the sequence

$$\bar{R}_z = \frac{\sum_{i=1}^{i^{th}} \sum_{j=1}^{j^{th}} |I[i,j]_1 - I[i,j]_{1+z}|}{n} \tag{3}$$

where I is a 8-bit gray-scale radiograph image with dimensions [i, j] and n is the total number of pixel elements ($i \times j$). Therefore, $\bar{R}_z$ is the forward piecewise average absolute difference of pixel intensity values between radiograph 1 (sample rotation = 0) and $1 + z$. We find that the average difference data ($\bar{R}_z$) over small angular rotations from 0.12° ($z = 1$) to 0.60° ($z = 5$) are minimal (see Figure 4). Therefore, differencing of the radiograph data to identify fluid movement over a sequence range of 1–5 radiographs should be possible. This sequence range is equivalent to a time interval of 40–200 ms, which is similar to the time scale at which pore-scale displacement events are known to occur [*DiCarlo et al.*, 2003]. Presumably, this result would differ for rock samples with different grain sizes, mineralogy, and grain shape and would have to be measured on a case-by-case basis to evaluate over what time scale the radiograph data could be sampled.

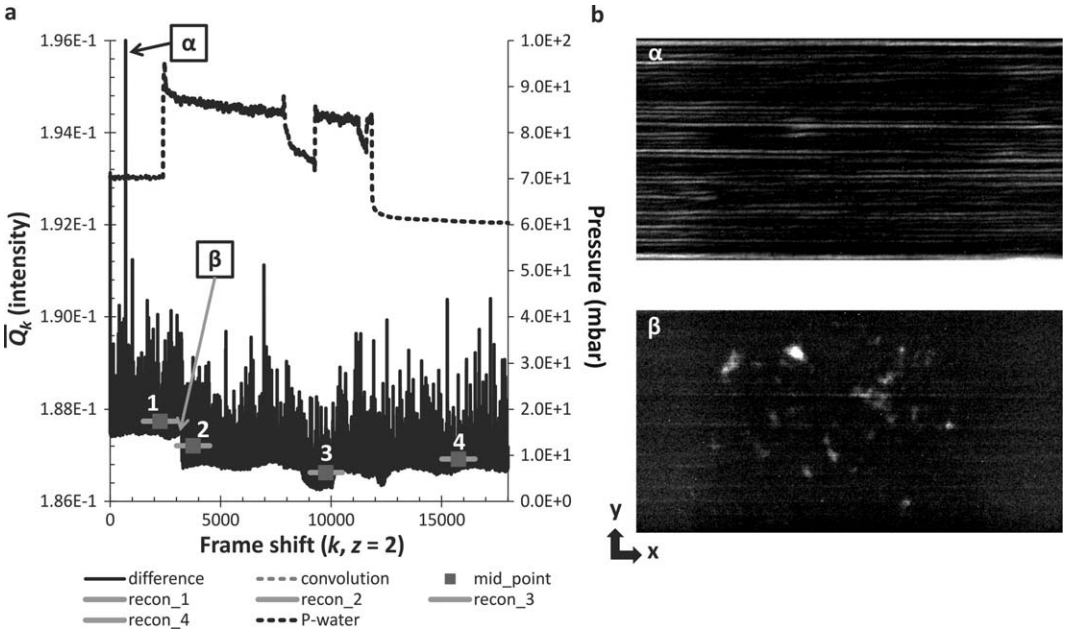

Figure 5. $\bar{Q}_k$ with $z = 2$ (a), the reconstructed data sets are the same as those presented in Figure 2b. Blurring artifacts occur in the reconstructed data when there is an average change in $\bar{Q}_k$ for a given reconstruction volume (see convolution data). However, $\bar{Q}_k$ is not sensitive to individual fluid-fluid displacement events since the signal-to-noise ratio is rather large. At point α, fluctuations in X-ray beam intensity results in a large $\bar{Q}_k$. At point β, fluid-fluid displacement events result in comparably smaller $\bar{Q}_k$. The same 8-bit gray-scale map was used to display both images (b).

The radiograph data sampled using equation (1) with $z = 2$ are presented in Figure 5 (this is equivalent to a time scale of 80 ms or a sample rotation of 0.24°). We also measured the data over 40 ms ($z = 1$), 120 ms ($z = 3$), and 160 ms ($z = 4$) and after analyzing the images decided that the most significant changes occurred at the 80 ms interval. However, the chosen differencing interval would depend on pore geometry, interfacial tension, and fluid viscosity. For a better understanding of how the rate at which a pore drainage event occurs is influenced by these parameters, see R. T. Armstrong et al. (submitted manuscript, 2014). Referring to Figure 5a, $\bar{Q}_k$ are reported as a dark black line, $\langle \bar{Q} \rangle_k$ are reported as a gray-dashed line (labeled by the term convolution), and the short solid gray lines represent the reading frames used to reconstruct volumes 1, 2, 3, and 4 that are presented in Figure 2b. In Figure 5a, both large fluctuations and average trends are apparent, as marked by symbols α and β, respectively. By analyzing the convolution data ($\langle \bar{Q} \rangle_k$) and the resulting reconstruction volumes, it is evident that when a large change in $\langle \bar{Q} \rangle_k$ occurs the streaking artifacts are visually present. However, the measurement was not sensitive to individual fluid-fluid displacement events since there were too many high-frequency fluctuations in the difference data ($\bar{Q}_k$). The question is now what causes these high-frequency fluctuations, i.e., whether they are results of a fluid-fluid rearrangement or rather imaging artifacts. In Figure 5b, we present the difference images (D_k) prior to calculating $\bar{Q}_k$

$$D_k = |I[i,j]_k - I[i,j]_{k+2}| \tag{4}$$

where D_k is the forward absolute difference between radiograph k and radiograph $k + 2$. At point α, we observe bright horizontal stripes, which are likely caused by fluctuations in X-ray beam intensity that apparently occurs over the 80 ms time scale. These stripes result in large $\bar{Q}_k$ values that are not associated with fluid flow. At point β, the observed bright spots that visually correlate with the known shape and size of pores are evidence of fluid-fluid displacement events, which result in a smaller $\bar{Q}_k$ value. Note that the beam fluctuations associated with the horizontal stripes were robust against the normalization filter (see materials and methods) applied to the radiograph data before calculating the difference images. Overall, the presented results demonstrate that the signal-to-noise for measuring fluid-fluid displacement events by taking average absolute differences is far from optimal because of fluctuations in X-ray beam intensities that occur over a time scale similar to the displacement events, i.e., the separation in time scales is not given anymore. However, there is a separation in length scales since the relevant structures are unique to the typical sizes of a few pores.

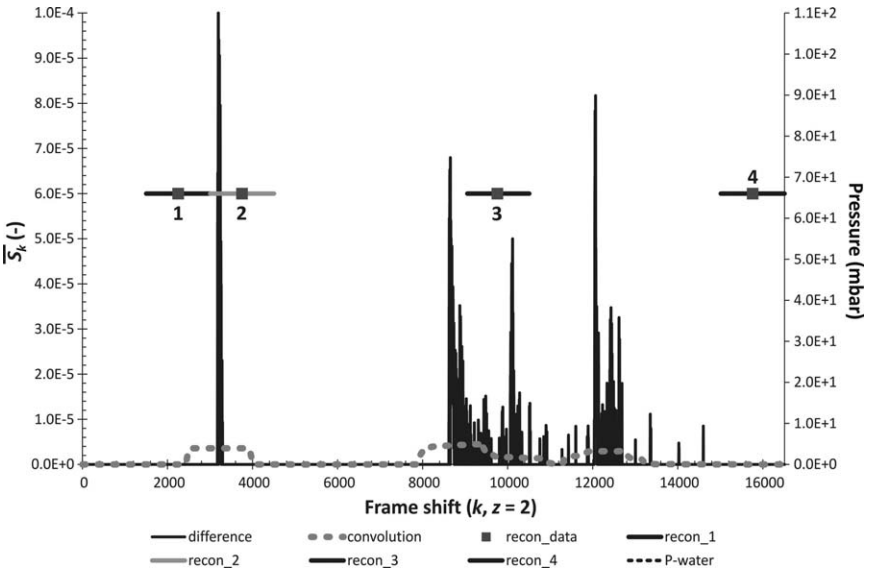

Figure 6. $\bar{S}_k$ for the segmented data; the reconstructed data sets are the same as those presented in Figure 2b. Clearly, the blurring artifact in the reconstructed data only occurs when displacement events occur during a scan.

Since the pore-scale events and the horizontal stripe artifacts have very different shapes and length scales, it might be possible to separate and filter the artifacts in the (spatial) frequency domain. To characterize the noise associated with the bright horizontal strips, we determined the power spectrum of the difference images (D_k). From the power spectrum data, we found that the bright horizontal strips and the fluid-fluid displacement events corresponded to different spatial frequencies and therefore, we were able to filter the D_k data with an FFT band-pass filter (see materials and methods) to remove the horizontal strips and highlight the displacement events. We then segmented the filtered D_k data using an active contours method (see materials and methods). The segmented difference data (S_k) are binary, with pixel values of 1 corresponding to regions in the radiograph data where displacements events occurred. We then calculate the piecewise average of S_k as

$$\bar{S}_k = \sum S_k[i,j]/n \tag{5}$$

where n is the total number of pixel elements ($i \times j$). Then by substituting $\bar{S}_k$ for $\bar{Q}_k$ in equation (2), the average $\bar{S}_k$ value $\langle \bar{S} \rangle_k$ for any given frame shift location k can be calculated. In Figure 6, $\bar{S}_k$ are reported as a dark black line, $\langle \bar{S} \rangle_k$ are reported as a gray-dashed line (labeled by the term convolution), and the short solid gray lines represent the reading frames used to reconstruct volumes 1, 2, 3, and 4 that are presented in Figure 2b. It is clear that no displacement events occurred during reconstruction volume 1 and therefore, the reconstruction data were artifact free. However, the pressure transducer measured a significant change in pressure during this time period, which could be a shortcoming in the experimental design or more likely that the pressure readings are sensitive to morphological changes that occur throughout the entire sample whereas the radiograph data provide information specific to the imaged region. In contrast, displacement events do occur during the collection of radiographs for reconstruction volume 2, which results in streaking and overall poor image quality. If reconstruction volume 2 was shifted forward in time by only a few 100 radiographs, then the displacement events could have been avoided and higher quality data could be reconstructed directly after the morphological changes occurred. Near radiograph 2500 ($k = 2500$), the fluid injection rate was increased by an order of magnitude and it is clear in Figure 6 that, after a short delay, displacement events occur. The small delay can be explained by the fact that the field of view for the collected radiographs was along the vertical center of the sample and therefore, any saturation change caused by increasing the fluid injection rate would require a brief lag period before it is observable.

In this section, the proposed qualifier function (equation (1)) with $z = 2$ worked well for identify pore scale displacement events at the millisecond time scale. However, because of single-to-noise problems the difference images of sequential radiographs had to be segmented prior to calculating $\bar{Q}_k$ and $\langle \bar{Q} \rangle_k$. Therefore,

the final qualifier function values, as reported in Figure 6, are referred to as $\bar{S}_k$ and $\langle \bar{S} \rangle_k$ to denote that the summation was performed on segmented images (see equations (4) and (5)). In the next section, we discuss methods to study the flow processes in regions of the radiograph data, as presented in Figure 6, where no artifact-free data could be reconstructed, i.e., regions where frequent morphological changes occur that resulted in relatively large and frequent $\bar{S}_k$ values.

3.3. Fluid Flow

In this section, our aim is to understand and quantify the fluid-fluid displacement events that occur between any two given reconstruction volumes. In the following paragraphs, we provide examples of how this is accomplished and can be used to study the different flow regimes that occur during fractional flow. In Figure 7, we present a comparison between the pore size distribution for the Robuglas® sample and the fluid-fluid displacement event-size distribution measured from the segmented difference data (S_k). The pore-size distribution was measured from the maximum inscribed balls pore extraction method, as provided by Imperial College London [*Dong and Blunt*, 2009] and adapted from the earlier work of *Silin and Patzek* [2006]. The volume of each event was inferred from the S_k data by measuring the effective radius of the events using the equation of a circle

$$r = \sqrt{A/\pi} \tag{6}$$

where A is the area of a connective region of pixels and r is the effective radius. We then apply the effective radius value to the equation of a sphere

$$V = \frac{4}{3}\pi r^3 \tag{7}$$

where V is event volume. This is likely an under estimate of the event size since the spatial morphology of nonwetting phase is known to be more branch-like than spherical. However, the results in Figure 7 are comparable to that presented in *Berg et al*. [2013a], where it was shown from pressure transducer readings that the most frequent drainage event sizes are larger than the average pore size. The results presented in Figure 7 provide validity to the results presented by *Berg et al*. [2013a] since herein the event sizes are measured directly from digital images rather than inferring that fluctuations in the pressure data correspond to drainage events, see *Yuan and Swanson* [1989], *Yuan* [1990, 1991], and *Morrow* [1970].

In addition to measuring event sizes, the order, frequency, and spatial location of displacement events can be measured using the S_k data. In Figure 8, we present displacement event data from the collected radiographs that correspond to events caused by increasing the pumping rate during the experiment. Figure 8a displays the size and order of events between radiograph 3170 and 3290 that correspond to a time interval of 3160 ms, which is divided into two intervals in Figures 8b and 8c. Initially, many small and large events occur when the flow rate is increased and then the system appears to stabilize to mostly larger events. For the presented time interval, fluid-fluid displacement events occur at an average rate of 268 events per second. These events can also be tracked in the *x-y* plane of the segmented radiograph data (Figures 8b and 8c). Of course, because of sample rotation the analyzed region of space will translate in the *x* direction; however, over short periods of time the

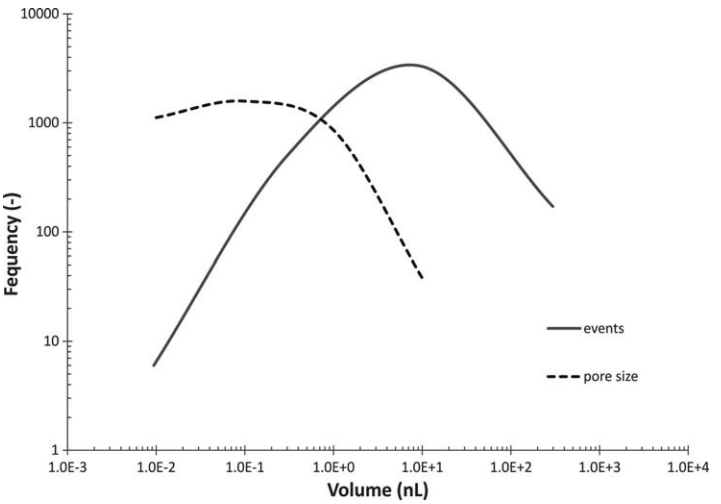

Figure 7. A comparison between the distribution of pore sizes and fluid-fluid displacement event sizes for the Robuglas® sample.

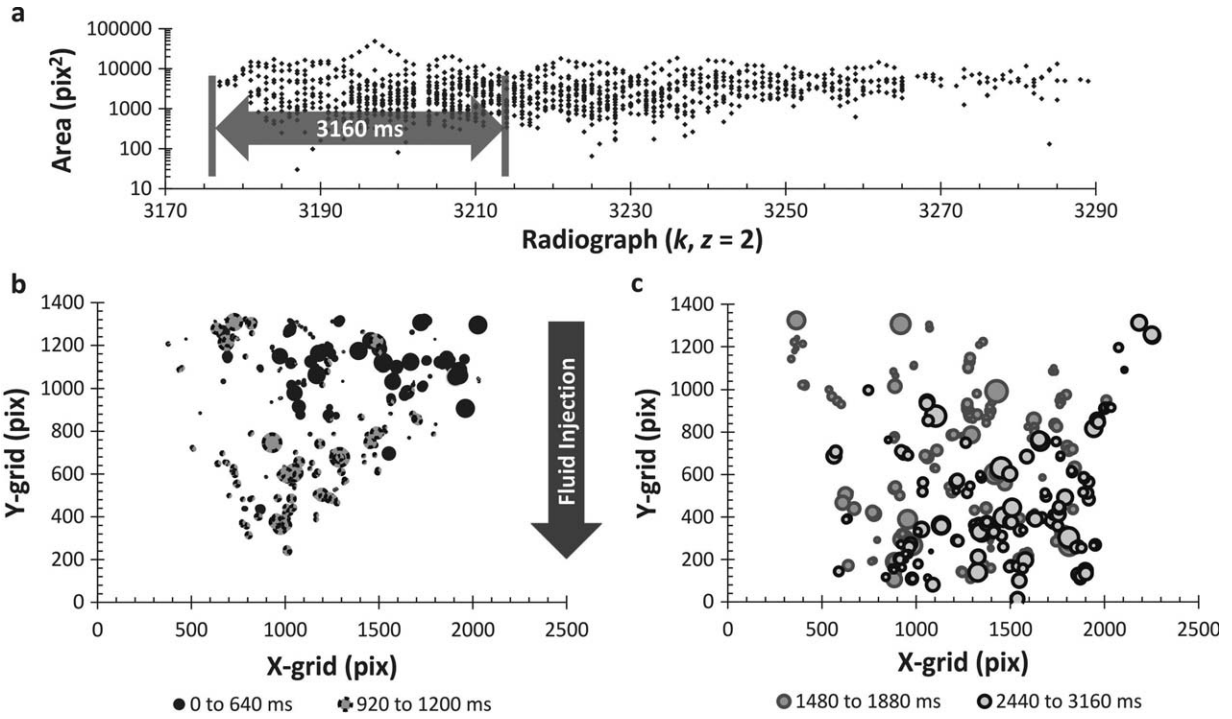

Figure 8. Event sizes measured from each segmented difference radiograph (a) and the location of each event in the *x-y* plane (b). The time interval analyzed is displayed in Figure 1b. In (b) each point corresponds to the location of a displacement event in the segmented X-Y projection and the size of the point corresponds to the relative event size.

translation is minimal. For example, the sample will rotate 30° in 10 s, which means that pore regions near the perimeter of the 4 mm diameter sample will translate by a maximum of 127 pixels in the *x* direction, which is less than 5% of the total X distance in the *x-y* plane. In Figure 8, the unsteady state movement of a saturation front is evident as the tracked locations of displacement events move steadily across the *x-y* plane in the *y* direction. This clearly indicates that an unsteady state flow condition occurs when the total injection rate is increased and F_w remains constant.

Data similar to Figure 8 are presented in Figures 9 and 10, which correspond to different time intervals during the fractional flow experiment (see Figure 1b). Figure 9 corresponds to an interval during the experiment where $F_w = 0.5$, $Q = 300$ $\mu l/min$, and there is no change in flow rate. During this interval between radiographs 8610 and 8790, a large pressure fluctuation occurs even though the pressure reading was relatively stable for the previous 6 min (since radiograph 3000). Similar to when the flow rate was increased, as displayed in Figure 8a, in Figure 9a displacement events start with a large variability in size and then the system appears to stabilize to mostly larger events. However, in contrast to Figure 8a, the frequency of events is much lower with an average rate of 99 events per second. Also, in Figure 9b there is no obvious movement of a saturation front across the field of view. Rather, displacement events appear to cluster in specific regions on the *x-y* plane. This pattern of events is likely more characteristic of steady state flow, where preferential pathways are established across the field of view and pore regions along the interface between the connected paths fluctuate between drainage and imbibition events.

In Figure 10, we present the time interval between radiographs 12,030 and 12,210, which correspond to when the fluid injection pumps were stopped. Once again, displacement events start with a large variability in size and then tend to larger and less frequent events, with an average event rate of 91 events per second (Figure 10a). In Figure 10b, for the first 8920 ms, displacement events move across the *x-y* plane in the *y* direction and then between 15,320 and 21,040 ms (Figure 10c) the events appear to be randomly distributed on the *x-y* plane. This is likely indicative of an unsteady state saturation front moving across the field of view caused by the stopping of the pumps. Then interfacial relaxation is likely to occur, where pores throughout the field of view tend to fluctuate between drainage and imbibition while the system approaches a local energy minimum.

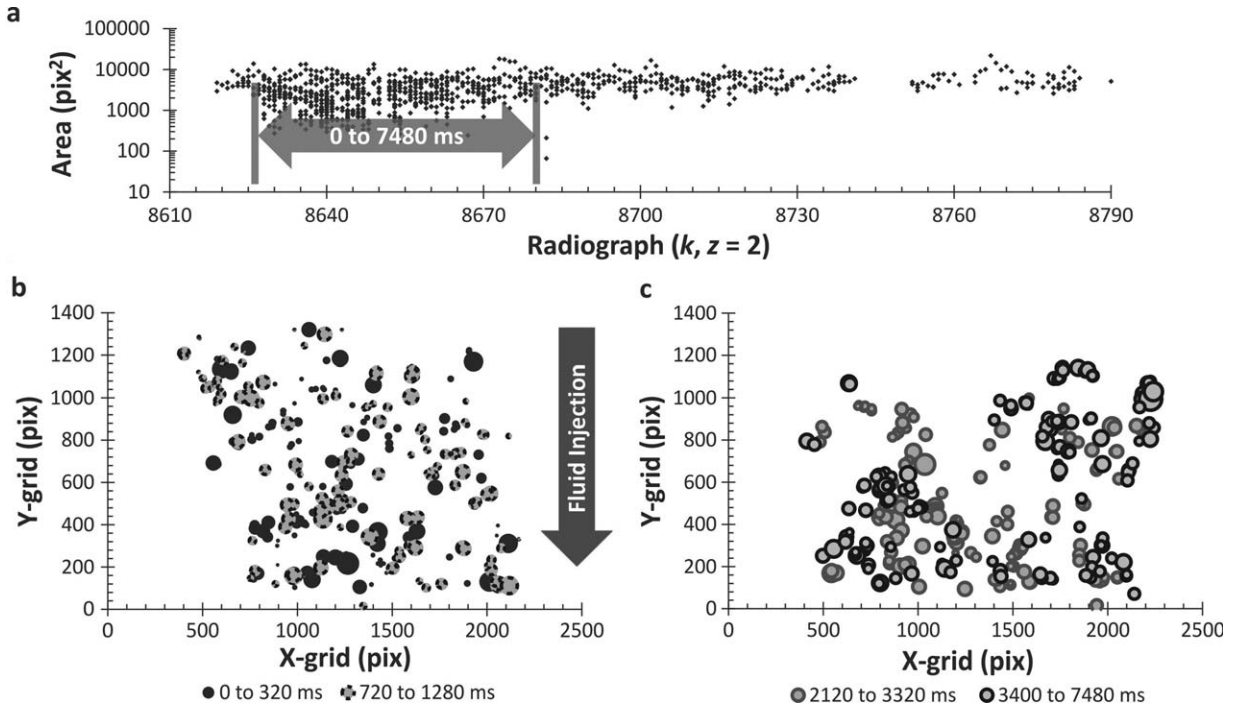

Figure 9. Event sizes measured from each segmented difference radiograph (a) and the location of each event in the *x-y* plane (b). The time interval analyzed is displayed in Figure 1b. In (b) each point corresponds to the location of a displacement event in the segmented X-Y projection and the size of the point corresponds to the relative event size.

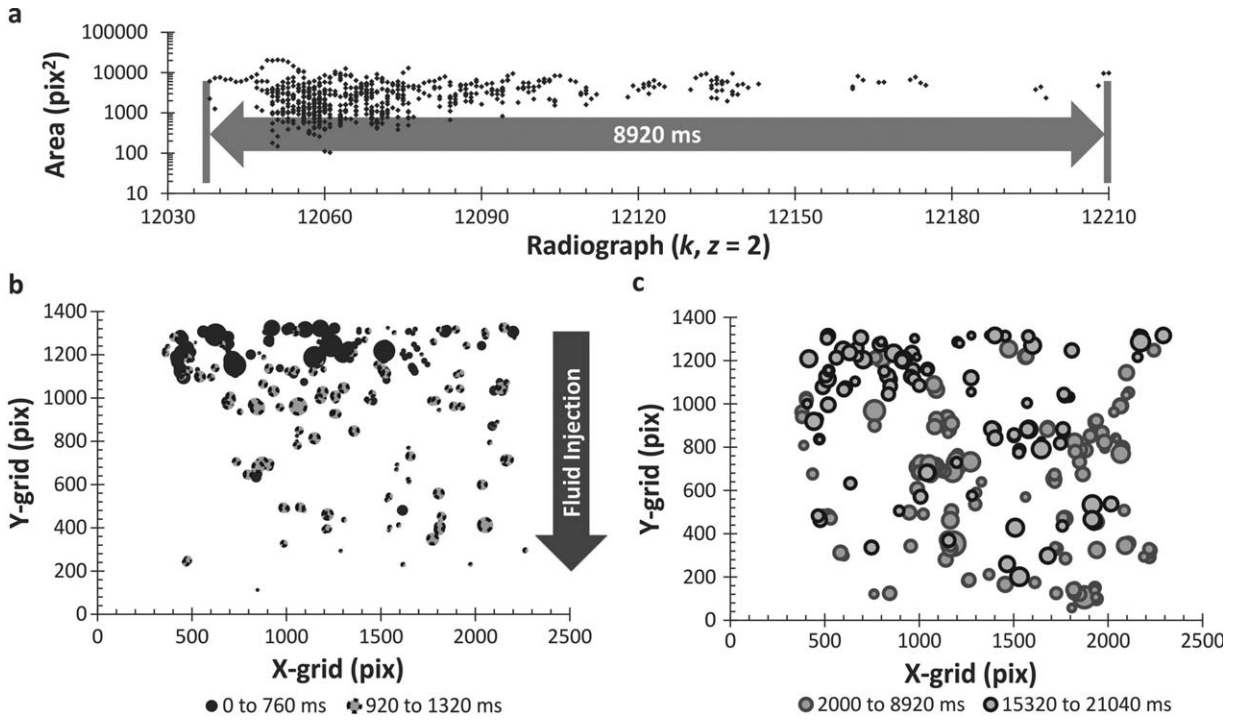

Figure 10. Event sizes measured from each segmented difference radiograph (a) and the location of each event in the *x-y* plane (b). The time interval analyzed is displayed in Figure 1b. In (b) each point corresponds to the location of a displacement event in the segmented X-Y projection and the size of the point corresponds to the relative event size.

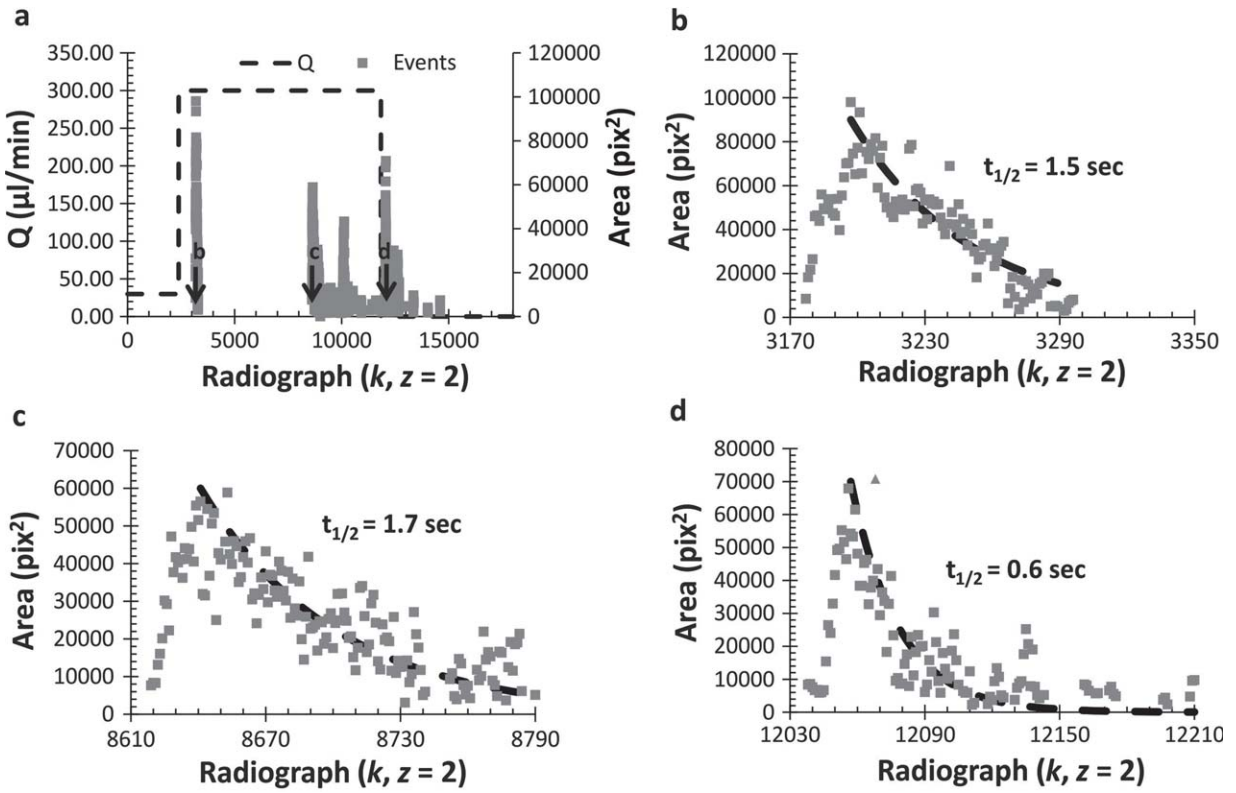

Figure 11. Sum of pore-scale events per radiograph (area) versus time (radiograph, *k*) and the total pumping rate (a). Zoomed in regions of the data when flow rate was increased (b), flow rate was constant (c), and flow rate was stopped (d). An exponential-like decay was observed in Figures 11(b)–11(d) indicating relaxation from an out-of-equilibrium state to a quasi equilibrium. An exponential decay was fitted to Figures 11(b)–11(d) with the characteristic decay time $t_{1/2}$ (when the initial value decreased to its half) showing faster relaxation to equilibrium after flow has been stopped (Figure 11d) compared to the dynamic flow situations in Figures 11(b) and 11(c).

In Figure 11, we explore how quickly the Robuglas® system responds to flow rate changes. The presented area value (pix^2) is a proxy to fluid flux, measured by summing the total area of displacement events per S_k (summation of all pixel values) and then plotting the summation ($\sum S_k$) versus radiograph number *k*. In other words, we binned the data from Figures 8a, 9a, and 10a over a 40 ms time interval, i.e., the radiograph exposure time. We observe that when a sequence of events occurs, the volume of fluid involved rapidly increases and then decays over a much longer time scale. The cascade of events includes a primary sequence and then a sequence of follow-up events through which some kind of relaxation mechanism to a new quasi-equilibrium state can be observed. Presumably, the volume of fluid displaced, from an initial event, must be redistributed over the local pore-space, which could trigger sequential events and the observed decay is a cascade of occurrences of fluid redistribution. Therefore, we speculate that the relaxation time could be indicative of fluid permeability at a given saturation. We can estimate the time scale of the decay by fitting the data to an exponential decay $e^{-\frac{t}{\tau}}$ and reporting the half-life ($t_{1/2} = \ln(2)\,\tau$) of the event sequences. During the experiment, the flow rate was increased, allowed time to approach steady state, and then stopped (Figure 11a) and the resulting response functions are presented in Figures 11b–11d, respectively. Independent of the flow rate manipulation the relaxation time ranges from 0.5 to 2.0 s. There appears to be a general trend that the relaxation time during flow is longer than when flow is stopped. For example, when stopping flow (changing low rate from 300 to 0 µL/min) results in a half-life of 0.6 s; whereas, an increase in flow rate change of 30–300 µL/min results in a half-life of 1.6 s. However, there are other possible reasons and further experiments with a statistically significant number of events would be required to understand the trends. The more general point is that we can measure the relaxation sequence and cooperative dynamics of pore-scale events in 3-D porous materials, which links to our previous work using micromodel systems with high-speed photography and pore-scale modeling to study the cooperative dynamics of immiscible fluid-fluid displacement in porous media [*Armstrong and Berg*, 2013] (R. T. Armstrong et al., submitted manuscript, 2014).

4. Conclusions

The aim of this article was to present a robust method that can be used to study pore-scale multiphase flow under dynamic flow conditions with fast-μCT and to provide new insights into the flow physics. The approach consists of analyzing the 2-D radiographs collected during a μCT scan to better understand pore-scale immiscible flow at the millisecond time scale and to identify time intervals where the highest quality 3-D images can be reconstructed. In this way, we extract a wealth of information from μCT data where no artifact-free data could be reconstructed because of frequent morphological changes during data collection. The extracted data allow for the study of immiscible fractional flow in porous media at the time and spatial scales necessary to understand pore-scale fluid-fluid displacement processes. The following major findings were reported.

1. Fluid motion during a fast-μCT is manifested as streaking artifacts in the final reconstructed data.
2. Sequential radiograph data can be subtracted and segmented to identify the ideal regions in time for 3-D image reconstruction.
3. The radiograph data demonstrate that displacement events at the milliseconds time scale are larger than the average pore size.
4. Once a sequence of events is initiated, the total fluid flux involved decays exponentially over the time scale of approximately 1 s.
5. Presumably, the initial event is local involving a given volume of fluid displacement that is then redistributed over a larger range. Therefore, the observed decay in fluid flux could be related to sample permeability.
6. We are able to observe a more detailed structure of fluid-fluid displacement in both space and time than previously (40 ms versus 10–30 s).
7. The fluid front propagates in cascades that can be tracked in both space and time, which can be used to identify different flow regions (i.e., steady versus unsteady state).

Overall, this approach can be seen as a way to evaluate flow regimes in different rock types and thus, characterize rock types that could be the most suitable for a given engineering technology. Also, we envisage that a similar approach could be taken to validate pore-scale numerical rock simulations by assessing if the simulator captures the correct flow regimes when calculating the relative permeability of a given rock sample.

Acknowledgements
This work was performed at the Swiss Light Source, Paul Scherrer Institute, Villigen, Switzerland, in collaboration with the University of Mainz, Germany and Shell Global Solutions International. We gratefully acknowledge Ludwig Simon, Frieder Enzmann, Kevin Mader, and Marco Stampanoni for insightful discussions pertaining to the presented work. This work was supported by Shell Global Solutions International B.V. and to request data please contact Steffen Berg (steffen.berg@shell.com). We would also like to thank the Associate Editor and three Anonymous Reviewers for valuable advice in the revision of this manuscript.

References

Al-Raoush, R. I. (2009), Impact of wettability on pore-scale characteristics of residual nonaqueous phase liquids, *Environ. Sci. Technol.*, *43*(13), 4796–4801.

Armstrong, R. T., and S. Berg (2013), Interfacial velocities and capillary pressure gradients during *Haines* jumps, *Phys. Rev. E*, *88*(4), 043010.

Armstrong, R. T., Georgiadis, A., Ott, H., Klemin, D., and S. Berg (2014), Critical capillary number: Desaturation studied with fast X-ray computed microtomography, *Geophys. Res. Lett.*, *41*, 55–50, doi:10.1002/2013GL058075.

Avraam, D. G., and A. C. Payatakes (1995), Flow regimes and relative permeabilities during steady-state two-phase flow in porous media, *J. Fluid Mech.*, *293*, 207–236.

Berg, S., et al. (2013a), Real-time 3D imaging of Haines jumps in porous media flow, *Proc. Natl. Acad. Sci.*, *110*(10), 3755–3759.

Berg, S., et al. (2013b), Multiphase flow in porous rock images under dynamic flow conditions with fast X-ray computed tomography, in *International Symposium of Core Analysts, SCA2013-011*, Napa Valley, Calif., 16–19 September.

DiCarlo, D. A., Cidoncha, J. I. G., and C. Hickey (2003), Acoustic measurements of pore-scale displacements, *Geophys. Res. Lett.*, *30*(17), 1901, doi:10.1029/2003GL017811.

Dong, H., and M. J. Blunt (2009), Pore-network extraction from micro-computerized-tomography images, *Phys. Rev. E*, *80*, 036307, doi: 10.1103/PhysE.80.036307.

Haines, W. B. (1930), Studies in the physical properties of soil. V. The Hysteresis effect in capillary properties, and the modes of moisture distribution associated therewith, *J. Agric. Sci.*, *20*(97), 97–116.

Iglauer, S., A. Paluszny, C. H. Pentland, and M. J. Blunt (2011), Residual CO_2 imaged with X-ray micro-tomography, *Geophys. Res. Lett.*, *38*, L21403, doi:10.1029/2011GL049680.

Koroteev, D., et al. (2013), Direct hydrodynamic simulation of multiphase flow in porous rock, in *International Symposium of Core Analyst, SCA2013-014*, Napa Valley, Calif., 16–19 September.

Mohanty, K. K., H. T. Davis, and L. E. Scriven, (1987) Physics of oil entrapment in water-wet rock, *SPE Reservoir Eval. Eng.*, *2*(1), 113–128.

Morrow, N. (1970), Physics and thermodynamics of capillary action in porous media, *Ind. Eng. Chem.*, *62*(6), 32–56.

Myers, G. R., A. M. Kingston, T. K. Varslot, M. L. Turner, and A. Sheppard (2011), Dynamic tomography with a priori information, *Appl. Opt.*, *50*(20), 3685–3690.

Pentland, C. H., S. Al-Mansoori, S. Iglauer, B. Bijeljic, and M. J. Blunt (2010), Measurement of non-wetting phase trapping in sand packs, *SPEJ*, *15*(2), 274–281.

Silin, D., and T. Patzek (2006), Pore Space morphology analysis using maximal inscribed spheres, *Physica A*, *371*, 336–360.

Wildenschild D., J. W. Hopmans, C. M. P. Vaz, M. L. Rivers, D. Rikard, and B. S. B. Christensen (2002), Using x-ray computed tomography in hydrology: Systems, resolutions and limitations, *J. Hydrol.*, *267*, 285–297.

Wildenschild D., J. W. Hopmans, M. L. Rivers, and A. J. R. Kent (2005), Quantitative analysis of flow processes in a sand using synchrotron-based x-ray microtomography, *Vadose Zone J.*, *4*(1), 122–126.

Youssef, S., H. Deschamps, J. Dautriat, E. Rosenberg, R. Oughanem, E. Maire, and R. Mokso (2013), 4D imaging of fluid flow dynamics in natural porous media with ultra-fast X-ray microtomography, in *International Symposium of Core Analyst, SCA2013-012*, Napa Valley, Calif., 16–19 September.

Youssef, S., D. Bauer, S. Bekri, E. Rosenberg, and O. Vizika (2009), Towards a better understanding of multiphase flow in porous media: 3D in-situ fluid distribution imaging at the pore scale. International Symposium of the Society of Core Analysts, Noordwijk, Netherlands, 27–30 September, 2009, SCA2009-17, pp 1–12. [Available at www.scaweb.org/search.shtml.]

Yuan, H. (1990), Advances in APEX Technology, in *Society of Core Analysts, Fourth Annual Technical Conference*, 15–16 August.

Yuan, H. (1991), Pore-scale heterogeneity from mercury porosimetry data, *SPE Form. Eval.*, *6*(2), 233–240.

Yuan, H., and B. F. Swanson (1989), Resolving pore-space characteristics by rate-controlled porosimetry, *SPE Form. Eval.*, *4*(1), 17–24.